Journal of Power Sources 188 (2009) 578–582

Contents lists available at ScienceDirect

Journal of Power Sources

journal homepage: www.elsevier.com/locate/jpowsour

Short communication

High rate capability pure Sn-based nano-architectured electrode assembly for rechargeable lithium batteries

L. Bazin[a], S. Mitra[a], P.L. Taberna[a], P. Poizot[b], M. Gressier[a], M.J. Menu[a], A. Barnabé[a], P. Simon[a,*], J.-M. Tarascon[b]

[a] CIRIMAT-UMR 5085- Université Paul Sabatier, route de Narbonne, 31062 Toulouse Cedex 4, France
[b] LRCS-UMR 6007-Université de Picardie Jules Verne, 33 rue Saint-Leu, 80039 Amiens, France

ARTICLE INFO

Article history:
Received 20 June 2008
Received in revised form
12 November 2008
Accepted 8 December 2008
Available online 13 December 2008

Keywords:
Lithium-ion
Tin
Nanostructure
High rate
Electrolytic deposition
3D microbatteries

ABSTRACT

New high surface area nano-architectured copper current collectors have been designed based on simple electrodeposition method. The nano-architectured electrode design not only increases the effective surface area of the electrode but it is also very suitable for sustaining the mechanical and structural strain during electrochemical reaction. In this work, a nano-architectured Sn anode for Li-ion battery, based on Li–Sn alloying reaction, delivers very high cycle life and good power performance compared to planar tin films. This electrode could be successfully used in the field of 3D microbatteries.

1. Introduction

Recent advance of nanostructured materials has attracted much more attention in the field of supercapacitors [1] and high rate lithium-ion batteries [2,3]. Specifically, metal based (Sn, Sb and Si) [4] Li-ion batteries negative electrode are known to suffer from dramatic volumic expansion [5] during lithiation process. If the first method to overcome this drawback consist in using active material/inactive material alloys [6,7,8], in order to create a stable matrix to accommodate the strain, another promising way is to reduce the size of the active material [9,10,11]. In this topic, nanostructured materials can provide an interesting solution because, among others, of their adequate advantage in terms of mass transport. As an example, mass transport improvement leads to easy diffusion of lithium-ion thanks to shorter diffusion path, higher electrode/electrolyte interfacial contact area and better accommodation of structural strain associated with electrochemical intercalation/deintercalation, conversion or alloying reactions. If nanomaterials are usually processed into electrodes that keep a small diffusion length as well as adequate electrical and mechanical contact, their practical use is still uncertain. Recently, Martin and co-workers reported the new electrode design of direct elaboration of nano-architectured electrode by growing active nanostructured materials onto planar current collectors [12]. Although these electrode architectures help to pave the way to design new electrode for lithium-ion battery technologies, especially for 3D nanobatteries, it fails to some extend to deliver high rate capacity electrodes when metal oxides as well as alloy materials are used. It is important to tackle this issue since these type of materials are very promising because of their higher lithium amount storage ability as compare to graphite.

Recently, we have demonstrated a unique electrode design consisting in nano-architectured copper current collectors grown onto planar copper surface covered with an electroactive material using simple cost effective electrodeposition method [13]. In our first report, we presented a new, but simple, two-step electrode fabrication process using Fe_3O_4 as active material and Cu nanopillars as current collector. This new design demonstrated a factor of sixfold improvement in power density over planar electrodes. But the large hysteresis voltage loop between charge–discharge cycle observed with these conversion reaction processes decreases the energy efficiency thus limiting today their use for larger scale energy applications. The decreasing of the hysteresis is one of the key issue and ongoing works are to find solutions to alleviate it.

Bi and Ni_3Sn_4 deposits have also been achieved onto these nanostructured current collectors [14,15] and those electrodes

* Corresponding author. Tel.: +33 561556802; fax: +33 561556163.
E-mail address: simon@chimie.ups-tlse.fr (P. Simon).

0378-7753/$ – see front matter © 2008 Elsevier B.V. All rights reserved.
doi:10.1016/j.jpowsour.2008.12.025

exhibited high rate capability. We report here results obtained with Cu nanopillars covered with pure tin. It is well-known that Li–Sn alloy suffers from a large volume expansion and constriction during charge–discharge cycling leading to mechanical disintegration and very poor cycle life [7,16,17]. Here, we try to take advantage of the nanostructuration of our electrodes to buffer the mechanical strains occurring during the cycling of tin with lithium, thanks to larger free space available for alloy–dealloying reactions. Also, the nanometric dimensions of electrode and current collector would allow faster electron and Li^+ ions diffusion, leading to improve electrochemical kinetics.

2. Experimental

2.1. Preparation of the nano-architectured Cu current collector

Cu nano-architectured current collectors were obtained using previously reported procedure [13]. Briefly, arrays of highly perpendicular copper nanopillars on copper disk substrate were prepared by pulsed cathodic electrodeposition through an alumina oxide membrane. The deposits are done on 2 cm^2, 150-μm thick, 99.9% Cu foils from Goodfellow from an electrolytic bath containing $CuSO_4{\cdot}5H_2O$ 100 g L^{-1}, $(NH_4)_2SO_4$ (Acros Organics) 20 g L^{-1} and diethyl-tri-amine (DETA, Acros Organics) 80 mL L^{-1} using an Arbin BT2000 potentiostat/galvanostat. Membranes were purchased from Whatman (Anodisc 47, reference 6809 5022). Prior to use, copper foils were mechanically polished, first with SiC paper then with 6, 3, 1 and 0.25 μm diamond suspension. The electrolytic cell assembly has been fully described in our previous work [13].

2.2. Tin plating bath

Sn-based Cu nano-architectured electrodes were obtained by simple electroplating of tin onto Cu nano-architectured current collectors. Simply, the cathodic electrodeposition of Sn was made from an electrolytic bath consisting of $SnCl_2$ 20 g L^{-1}, methyl-sulphonic acid 100 g L^{-1}, 2-naphthol 1 g L^{-1} and gelatine 1 g L^{-1}. All chemicals were purchased from Aldrich Chemicals, France, and used as received. Depositions were performed using an Arbin BT2000 potentiostat/galvanostat. After Sn deposition, the obtained anode was washed with distilled water and acetone successively and then placed under argon atmosphere to avoid oxidation.

2.3. Electrochemical characterizations

Electrochemical characterizations were carried out by galvanostatic mode using VMP-3 multichannel potentiostat/galvanostat (Biologic). Sn–Cu nano-architectured electrodes were assembled in coin-type cells (CR 2016) in an argon filled dry-box. Lithium foils were used as both counter and reference electrodes and were separated from the working electrode by a Whatman GF/D borosilicate glass fibre sheet soaked in 1 M $LiPF_6$ electrolyte solution (in EC:DMC/1:1 in mass ratio) from Ferro Corporation, USA. In this work, we chose to report the capacitance of our electrodes in mAh cm^{-2}, area being footprint area of the electrode, since the applications for this nanostructured electrode would be mainly 3D microbatteries.

3. Result and discussions

Electroplating of Sn onto Cu nanopillars was achieved by pulsed cathodic current technique. A stacked two electrodes cell using a tin anode was used. Tin depositions were done at 25 °C on Cu pillars by two different pulsed current step conditions:

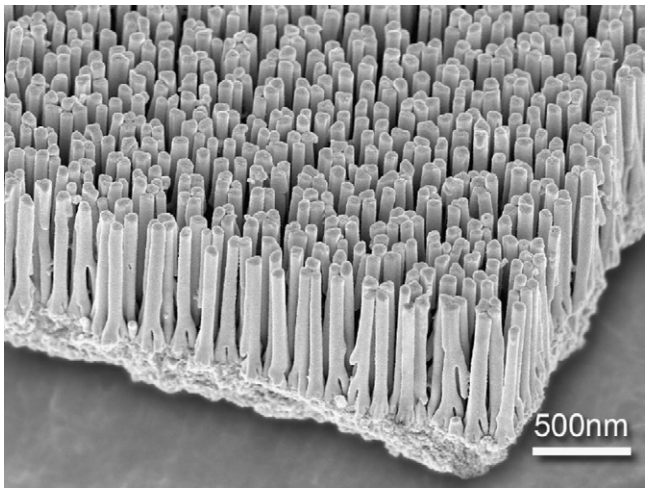

Fig. 1. SEM image of an as-deposited copper nanostructure.

- Step 1: a cathodic current pulse of −25 mA cm^{-2} during 1 ms.
- Step 2: 9 ms of rest, i.e. open circuit.

The 2nd step of 9 ms rest is performed to decrease the concentration gradient from top to bottom parts of the nanopillars due to species consumption during deposition. A systematic study was conducted on Cu nanopillar substrates using different electrodeposition times (3, 5, 10 and 15 min) to vary the amount of deposited tin.

Fig. 1 shows scanning micrograph (JEOL SEM) of an as-Prepared nano-architectured Cu current collector (cross-sectional view (Fig. 1a)). As observed, highly homogenous copper deposit was obtained. Cu pillars are perpendicular to the surface, 1800 nm height and 150–200 nm of diameter. Moreover, the inter-pillar distance was measured to be 150 nm.

Fig. 2a and b show scanning electron micrographs of as-deposited Sn–Cu nanopillar assemblies for two different deposition times (5 and 10 min) in top view. The shortest deposition time (5 min) shows a conformal covering Sn deposit on Cu nanopillar whereas increasing deposition time (10 min) leads to fully filled inter-pillar spaces. Fig. 2c shows TEM image of the 5 min deposited tin layer on the copper pillar. The thickness of this layer was measured between 20 and 50 nm, which is consistent with the SEM picture. Moreover, Fourier Transform treatment of the image indicates *d* spacing values of 3.75, 2.29 and 1.95 Å. According to PDF 00-005-0390, these inter-planar distances correspond to pure alpha tin ((1 1 1), (2 2 0), (3 1 1)).

Electrochemical tests were conducted, using the Cu nanopillars–Sn deposited assembly as positive electrode and Li metal as negative electrode. All cells were cycled between 1.8 and 0.02 V. Fig. 3a shows a typical potential versus capacity plots for the 3 and 5 min tin deposit samples. Same behavior was observed for all of tested samples, with the presence of several voltage plateaus over the first discharge. At a discharge rate of C/10, these plateaus are characteristics of the tin alloying with Li as previously described in various studies [18–21] according to the reaction (1)

$$\mathrm{Sn} + x\mathrm{Li} + + x\acute{e} \leftrightarrows \mathrm{Li}_x\mathrm{Snwith0} \le x \le 4.4 \quad (1)$$

Fig. 3b shows 2nd to 4th cycles of the 5-min Sn deposit sample. It can be seen at the second discharge cycle a hump at about 1.6 V that disappears during the following two cycles. In their study of a planar Cu electrode covered with electrochemical Sn deposit, Dahn's group attributed this hump to the decomposition of the electrolyte during the early stage of the discharge (lithiation) catalyzed by nano-sized tin particles produced during charge (de-lithiation)

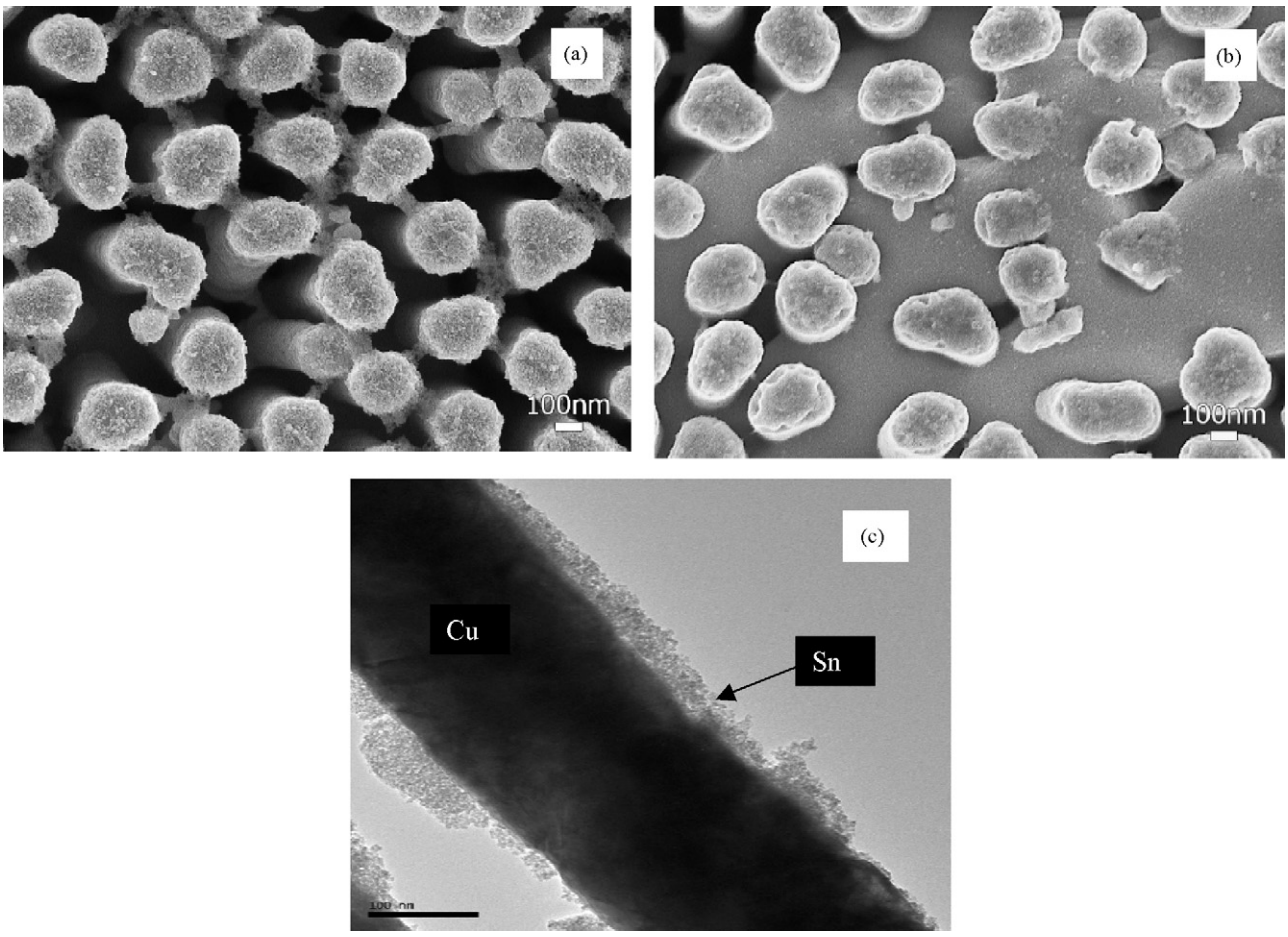

Fig. 2. (a) SEM image of Sn-covered Cu nanostructure 5 min deposition (top view), (b) SEM image Sn-covered Cu nanostructure 10 min deposition (top view) and (c) TEM picture of a single Sn-covered Cu nanopillar (5 min tin deposition).

when the voltage was increased above 1.6 V [21]. This decomposition led to a huge capacity decrease during the following cycle, due to the deactivation of the surface of tin particles covered by electrolyte decomposition by-products. In the present work, the cut-off voltage was 2 V; that explains the presence of the 1.6 V plateau in Fig. 3b.

Curves for cycles 3 and 4 give the same electrochemical signature as the curves obtained by Dahn's group in the case of pure Cu_6Sn_5 (figures 6 and 7 of ref. [21]). This identical electrochemical behavior, also found in several references [22–24] led us to propose that the plateau at 0.4 V during discharge can be assigned this to the formation of Li_2CuSn from Cu_6Sn_5/Li alloys. According to this, we believe that our electrode contains Cu_6Sn_5 formed during electrodeposition process. XRD experiments were conducted on the electrode to try to confirm. However, the thinness of the electrode as well as the particular geometry of the current collector made difficult the identification of Cu_6Sn_5.

Fig. 4 compares the specific capacity (mAh cm^{-2}) changes with cycling number for two cells assembled with planar and nanostructured *electrodes* covered by tin film, both obtained after 5 min deposition time. Cycling rate is C/2.

The initial capacity is in the same range for both electrodes, since the same deposition time was used for the planar and the nano-architectured electrode. The slight difference observed could be explained by the differences in the accessibility in the nano-architectured electrode that may affect in a small extend the coulombic efficiency at the bottom of the pores.

The capacity behavior of the planar electrode follows a well-known trend previously observed and described by many authors, with a sharp and constant decrease associated with huge volume expansion when moving from pure Sn to Li_xSn alloy [25–27]. The capacity retention of the nanostructured Cu–Sn electrode behaves differently. After an important decrease during first cycles, capacity stabilizes near 0.02 mAh cm^{-2}.

The capacity change with the cycle number highlights the merit of the nanostructured electrode design over flat surface configuration, overcoming the well-known cycling difficulties associated to mechanical disintegration resulting from the extreme volume change during Sn–Li alloying. This is explained by the nanostructure of the electrode. Keeping the tin amount constant, the high surface area developed by this electrode as compared to planar allows deposition of thinner Sn layer on the surface.

It is know that Sn–Cu can form alloy at room temperature [28]. Here, as previously shown in Fig. 3b, the electrochemical signature of Cu_6Sn_5 alloy is clearly visible at 0.4 V with nanostructured samples. Accordingly, we can propose that Cu_6Sn_5 alloy is formed at the high surface area Cu current collector/Sn interface. The presence of this Cu–Sn alloy conferred high capacity retention during cycling, acting as a mechanical buffer to limit the volume expansion during Li alloying into tin [21]. During the first cycle, the electrolyte decomposition occurs onto the Sn nano-particles that have not been alloyed with Cu; then, subsequent cycling mainly involves Cu_6Sn_5 alloy thin film, explaining the outstanding capacity retention observed for self supported Sn/Cu architecture, with 500 cycles with stable capacity of 0.02 mAh cm^{-2}.

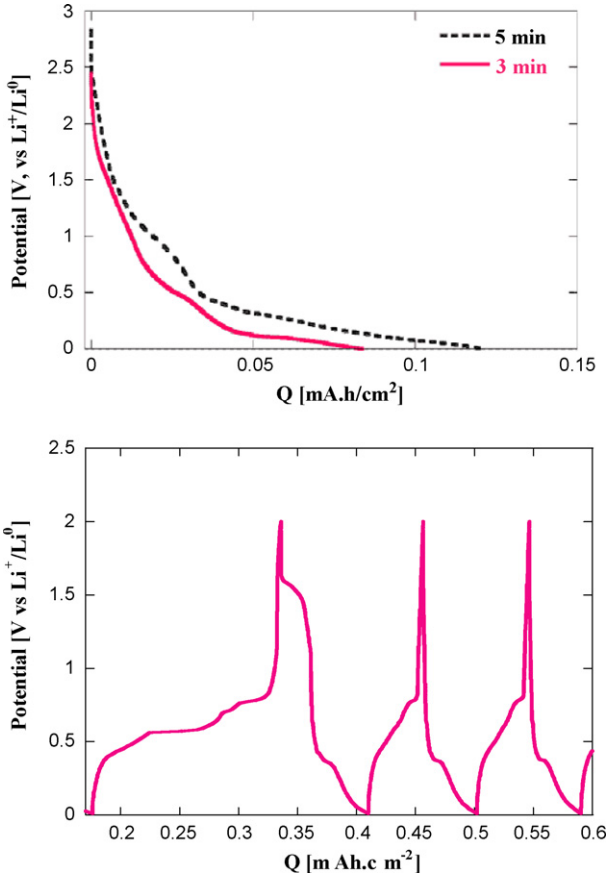

Fig. 3. (a) First discharge curve for 3 and 5 min deposition samples (cycling between 1.8 and 0.02 V, $I = C/10$); (b) cycles 2, 3 and 4 for 5 min deposition samples.

Fig. 5 presents a comparison of cycling behavior (specific capacitance) for cells assembled with planar and nanostructured electrodes.

Nanostructured electrode is obtained after a 5 min deposition of Sn while planar electrode is covered only with a very thin film of Sn (1 min deposition). These different deposition times should lead to the same film thickness on both electrodes, because of their different surface area.

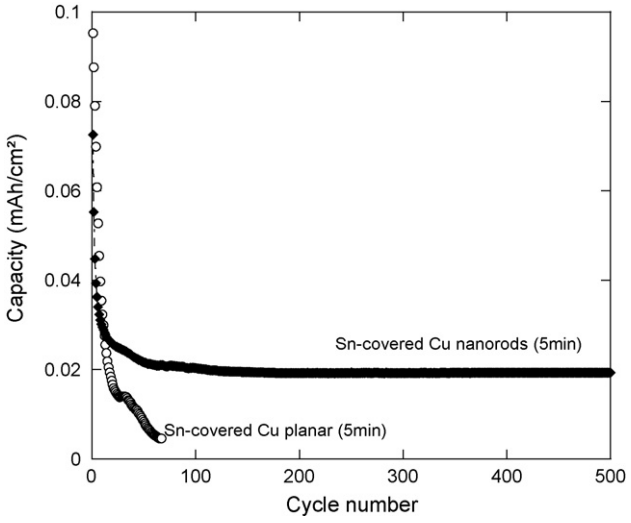

Fig. 4. Cycling performance of 5 min tin-covered nanostructure and planar Cu electrodes (5 min).

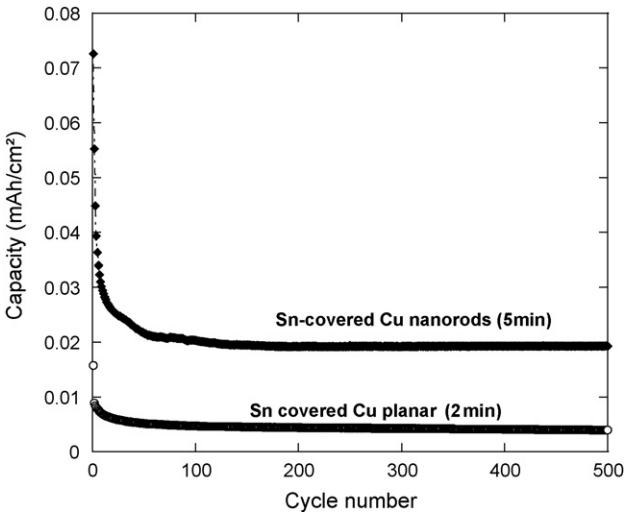

Fig. 5. Cycling performance of 5 min tin-covered nanostructure and planar (1 min).

Initial capacities indicate that the tin loading is much lower for the planar electrode than for the nanostructured one. This is consistent with the deposition time.

The thin-deposited planar electrode shows stability for 500 cycles with a very small capacitance of 4 μAh cm^{-2}. This stability can be explained by the thinness of the tin layer, allowing better accommodation of the volume change during cycling and faster kinetics. However, this value is five times less than the one obtained from the nanostructured electrode.

These results tend to confirm that the nano-architectured electrode is covered with a very thin film of Cu_6Sn_5 alloy at the Cu collector/Sn interface. Thanks to the thin alloy thickness, this electrode does not suffer from important mechanical stress during cycling and maintain its integrity. However, thanks to the large surface area developed by the nano-architectured electrode, it can be seen that reversible specific capacitance is five times higher. This value is consistent with the projected surface developed by the nanostructure (≈8 cm^2/cm^2). In other terms, cycling stability can be achieved with nanostructured electrode containing an active material loading five times superior to a stable planar electrode. This demonstrates the usefulness of such nano-architectured design for increasing the energy density while keeping high capacity retention during cycling.

The 5 min deposited Sn nano-architectured electrode and a 1 min deposited Sn planar electrode were tested for rate capability according to a protocol developed for lithium-ion battery technology called "Signature plot" [29]. Signature curves were collected on charge cycle, using cut-off voltage of 2 V for cells stopped after their third discharge to 0 V at low current rate (1 Li^+ in 5 h). As an example, we discharged the cell down to 0 V and recharged up to 2.0 V and discharged with same current rate. After two cycles of charge and discharge, we used a charge current of $j_1 = 0.255$ mA cm^{-2} (10 C) to charge cut-off potential of 2.0 V versus Li^+/Li. As soon as cell has reached 2.0 V, the cell delivered the capacity Q_1 and it was automatically kept under open circuit potential for 30 s. Then, the same charge was repeated, current being divided by 2: $j_2 = 0.120$ mA cm^{-2} (≈6 C), leading to the value of Q_2. Capacity Q_n was calculated by cumulating the measured capacity for each previous step: $Q_{6C} = Q_1 + Q_2$. Afterwards, the same strategy was used to calculate capacities under 0.06 mA cm^{-2} (≈3 C), 0.030 mA cm^{-2} (≈1.5 C), 0.015 mA cm^{-2} (≈0.75 C), 0.008 mA cm^{-2} (≈C/2), 0.004 mA cm^{-2} (≈C/4), 0.002 mA cm^{-2} (≈C/8) and 0.001 mA cm^{-2} (≈C/16), respectively.

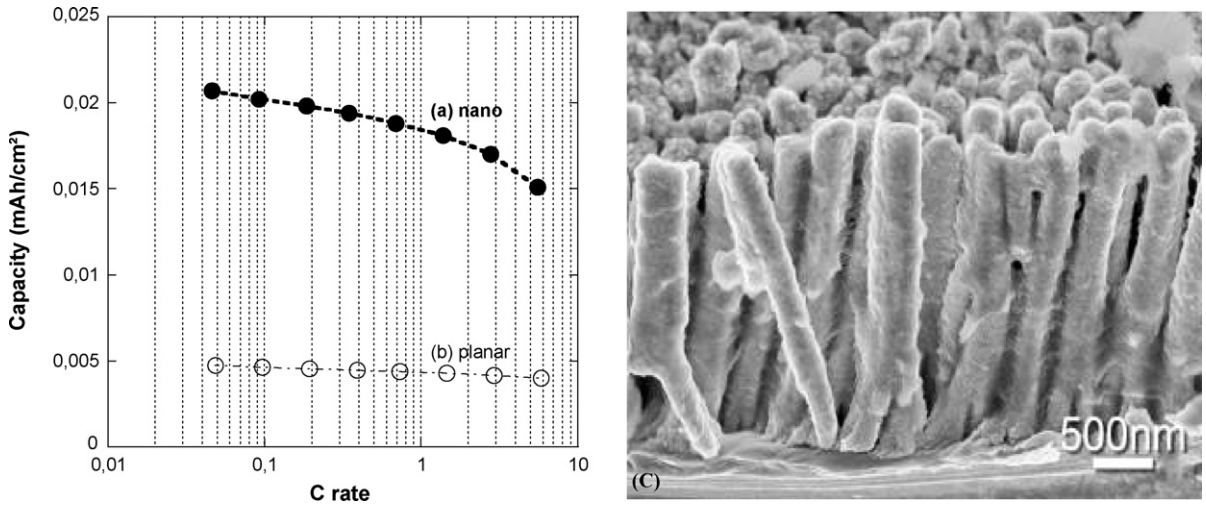

Fig. 6. Power plot of (a) Sn-coated Cu nanopillars and (b) Sn planat thin layer. (c) SEM image of the electrode after cycling.

Fig. 6a shows the variation of the cell capacity as a function of the applied rate expressed in terms of C, 1 C corresponds to the complete discharge of the cell in 1 h. Good rate capacity is observed for the nano-architectured electrode, giving a capacity retention of 75% between C/16 and 6 C, thus indicating the merit of the nano-architectured electrode design over flat surface. After being "power" then "cycle life" tested (100 cycles at high rate), the same nano-architectured electrode was observed using scanning electron microscope. It was observed that the Sn-based active material layer still stuck on the Cu nanopillar surface (Fig. 6b) and no appreciable change in morphology could be noticed. Considering the cycling stability (the signature of Cu_6Sn_5 is still visible after hundreds of cycles), we can also consider that the Cu_6Sn_5 layer maintained its integrity.

4. Conclusions

The significance of these results is a demonstration that outstanding power capability and capacity retention can be obtained from Sn–Li alloy-based nano-architectured negative electrode for lithium-ion battery. The observed cycle life (more than 500 cycles) and the power rate performances (75% of the capacity retained from C/16 and 6C) are both impressive. This is also another proof of the advantage of the nanorods shape for Li-ion anode. This brush-like morphology was proved to be an efficient way to accommodate mechanical strain during cycling in addition to display a large and accessible surface area. This nanostructured design makes possible the assembly of new 3D microbatteries, with enhanced energy density compared to 2D design.

Acknowledgement

The authors would like to thank the European Commission for the funding of this work achieved within the ALISTORE Network of Excellence.

References

[1] J. Chmiola, G. Yushin, Y. Gogotsi, C. Portet, P. Simon, P.L. Taberna, Science 313 (2006 1760).
[2] A.S. Aricò, P. Bruce, B. Scrosati, J.M. Tarascon, Nat. Mater. 4 (2005) 366–377.
[3] Y. Wang, K. Takahashi, K. Lee, G. Cao, Adv. Funct. Mater. 16 (9) (2006) 1133.
[4] T. Brousse, O. Crosnier, X. Devaux, P. Paillard, J. Santos-Pena, D.M. Schleich, Powder Technol. 128 (2002) 124.
[5] Z.H. Chen, V. Chevrier, L. Christensen, J.R. Dahn, Electrochem. Solid State Lett. 7 (10) (2004) A310.
[6] Finke, P. Poizot, GueryF C., J.M. Tarascon, J. Electrochem. Soc. 152 (12) (2005) A2364.
[7] S.D. Beattie, J.R. Dahn, J. Electrochem. Soc. 150 (7) (2003) A894.
[8] J. Hassoun, S. Panero, B. Scrosati, J. Power Sources 160 (2) (2006) 1336.
[9] A.H. Whitehead, J.M. Elliott, J.R. Owen, J. Power Sources 81–82 (1999) 33.
[10] O. Crosnier, T. Brousse, X. Devaux, P. Fragnaud, D.M. Schleich, J. Power Sources 94 (2001) 169.
[11] C. Kim, M. Noh, M. Choi, J. Cho, B. Park, Chem. Mater. 17 (2005) 3297.
[12] N. Li, C. Martin, B. Scrosati, J. Power Sources 97–98 (2001) 240.
[13] P.L. Taberna, S. Mitra, P. Poizot, P. Simon, J.-M. Tarascon, Nat. Mater. 5 (2006) 567.
[14] J. Hassoun, S. Panero, P. Simon, P.L. Taberna, B. Scrosati, Adv. Mater. 19 (12) (2007) 1632.
[15] A. Finke, P. Poizot, C. Guery, L. Dupont, P.L. Taberna, P. Simon, J.M. Tarascon, Electrochem. Solid State J. 11 (3) (2008) E5.
[16] N. Tamura, R. Ohshita, M. Fujimoto, M. Kamino, J. Fujitani, Electrochem. Soc. 150 (2003) A679.
[17] J.T. Li, S.R. Chen, X.Y. Fan, L. Huang, S.G. Sun, Langmuir 23 (26) (2007) 13174.
[18] M. Winter, J.O. Besenhard, Electrochim. Acta 45 (1999) 31.
[19] J. Chouvin, J. Olivier-Fourcade, J.C. Jumas, B. Simon, O. Godiveau, Chem. Phys. Lett. 308 (1999) 413.
[20] R. Retoux, T. Brousse, D.M. Schleich, J. Electrochem. Soc. 146 (7) (1999) 2472.
[21] S.D. Beattie, T. Hatchard, A. Bonakdarpour, K.C. Hewitt, J.R. Dahn, J. Electrochem. Soc. 150 (6) (2003) A701.
[22] S. Naille, R. Dedryvere, H. Martinez, S. Leroy, P.-E. Lippens, J.-C. Jumas, D. Gonbeau, J. Power Sources 174 (2007 1086).
[23] D. Larcher, L.Y. Beaulieu, D.D. MacNeil, J.R. Dahn, J. Electrochem. Soc. 147 (5) (2000) 1658.
[24] W. Choi, J.Y. Lee, H.S. Lim, Electrochem. Commun. 6 (2004) 816.
[25] Z.H. Chen, L. Christensen, J.R. Dahn, Electrochem. Commun. 5 (11) (2003) 919.
[26] N. Li, C. Martin, B. Scrosati, Electrochemical, Solid State Lett. 3 (7) (2000) 316.
[27] B. Scrosati, Electrochim. Acta 45 (15) (2000) 246.
[28] A. Finke, P. Poizot, C. Guery, J. Electrochem. Soc. 152 (2005) A2364.
[29] M. Doyle, J. Newman, J. Reimers, J. Power Sources 52 (1994) 211.